

# Apodizable Integrated Filters for Coarse WDM and FTTH-Type Applications

D. Iazikov, *Member, IEEE*, C. Greiner, *Member, IEEE, Member, OSA*, and T. W. Mossberg, *Member, IEEE, Fellow, OSA*

**Abstract**—A dual-channel integrated multiplexer, based on holographic Bragg reflector (HBR) devices and exhibiting flat-top, 4-nm-wide channels is demonstrated. Theory calibrated by the achieved performance indicates that HBR waveguide grating devices can be implemented to provide fully integrated and high-performance multiplexer solutions for CWDM and FTTH applications.

**Index Terms**—Apodization, coarse WDM (CWDM), fiber-to-the-home (FTTH), flat-top filter, holographic Bragg reflectors, mode-specific photonic bandgap, nanophotonics, photonic crystal, planar hologram, planar lightwave circuits.

## I. INTRODUCTION

THE development of inexpensive yet robust and high-performance optical multiplexing filters for datacom, coarse WDM (CWDM) and fiber-to-the-home (FTTH) applications poses an exciting challenge and opportunity to the optical community. We recently reported on a promising building-block element for distributed photonic circuits, which we refer to as a holographic Bragg reflector (HBR) [1], [2]. HBRs combine the best features of thin film filters (TFFs), fiber Bragg gratings (FBGs) [3]–[5], as well as monolithically integrated devices such as arrayed-waveguide gratings (AWGs) [6] and lattice-form filters [7] while avoiding many of their limitations. FBGs and TFFs offer powerful, potentially channel-specific passband control, but typically lead to assembled systems of daisy-chained discrete filters. Package size and fabrication complexity of such assembled systems increases drastically with the number of channels involved. Furthermore, the footprint of assembled packages is limited by the approximately  $2''$  minimum bending diameter required for long-term mechanical reliability of standard telecom interconnection fiber. Compact four-channel CWDM with stacked TFFs were recently reported [8] and avoid such limitations at the expense of higher insertion loss and lower isolation. Monolithically integrated multiplexers, such as AWGs, have attracted wide attention due to their compactness and batch-fabrication potential, fuelling numerous advances in planar lightwave circuit (PLC) fabrication [9]. AWGs are integrated and well suited to provide large numbers of identical channels, but do not lend themselves to flexible passband tailoring. Efforts to flatten their passband typically result in an increase in insertion loss of several dB, making such devices nonideal for wideband flat-top filter applications. Lattice-form-filter-based four-channel CWDM

with good isolation and tractable insertion loss has also been demonstrated [7]. However, such filters require multistage Mach-Zender interferometers (16 stages were used in [7]), and the complexity, size and fabrication sensitivity of the filters increase drastically with the number of the multiplexed channels. In contrast, HBR multiplexing technology is indeed both integrated, easily scales with the number of channels and provides passband control potentially as powerful as or superior to that of FBGs and TFFs. Flat-top, wideband, HBR-based filters may still have close to 100% passband reflectivity in a very compact footprint and, therefore, are especially well suited for CWDM and FTTH-type applications. An important advantage of HBRs is their full compatibility with straightforward mature PLC fabrication and packaging techniques.

The HBR devices demonstrated here (see Fig. 1) comprise two-channel multiplexing devices having flat-top, 4-nm-wide, channel passbands implemented on a  $1 \times 5 \times 32$  mm (thickness  $\times$  width  $\times$  length) silica-on-silicon optical chip. Device simulations, incorporating the present results and easily achievable enhancements in HBR structure, indicate that HBR-based, CWDM multiplexers having 16 channels, 13-nm flat-top passbands, and 1–2 dB fiber-coupled insertion loss should ultimately be obtainable on a die 5 mm  $\times$  20 mm in size. Since the HBR format is consistent with low-cost stamping/embossing-based fabrication, HBR-type CWDM and FTTH components (e.g., triplexers) may ultimately be provided at uniquely low costs.

## II. HBR DEVICES

The term holographic tends to be applied somewhat loosely in the literature. Often, use of the term holographic to describe a device implies more about the means by which the device was fabricated (interferometric optical exposure) than the device's function. HBRs are holographic in function. This means that the devices themselves comprise volume holograms (even though they are typically fabricated by noninterferometric means). A general volume hologram has powerful capability. In response to illumination by an input beam of specific spatial wavefront, the volume hologram can generate a predetermined output beam whose spatial wavefront is arbitrarily different. In fact, the diffractive contours of an HBR may be generally derived by computer simulated interference between an input signal beam and an output beam whose spatial wavefront is optimally configured for entry into an output port or other desired signal destination. The computer derived contour pattern may be exported to standard reticle generation software, utilized to generate a reticle, and fabricated via quarter-micron

Manuscript received November 5, 2003; revised January 7, 2004.

The authors are with LightSmyth Technologies, Inc., Eugene, OR 97401 (e-mail: diazikov@lightsmyth.com).

Digital Object Identifier 10.1109/JLT.2004.825352

resolution direct deep ultraviolet (DUV) photolithography (or equivalent means). At the same time, the volume hologram applies a spectral filtering function which is controlled by the hologram's detailed structure as a function of depth (along the waveguide in the present case). The ability of a hologram to effect complex spatial wavefront transformations is a significant advance over the elementary wavefront changes that can be implemented by simple conic-section diffractive surfaces. In some simple cases, such as paraxial, unity-conjugate-ratio imaging, exact holographic contours can be approximated by simple conic sections. In fact, the HBRs employed in the present case perform sufficiently simple imaging so that we can approximate diffractive contours with circular arcs. The arcs are not simple and regularly spaced, however. Each arc, as described below, is written in segments to control the diffractive amplitude and spatially displaced to introduce programmed phase shifts. The detailed spectral programming implemented in the present devices requires the same fabrication capability as required for general holographic imaging with diffractive contours of arbitrary shape. The powerful advantage of general holographic wavefront mapping will become apparent as HBR development continues. While the present devices utilize relatively simple contours, we refer to them as holographic to remind the reader of the demonstrated fabrication capability, enabled by accumulated advances in photolithographic tools, that allows a designer to utilize advanced optical wavefront handling concepts in the domain of integrated optics. HBRs may also be viewed as directional (or mode-specific) photonic bandgaps.

The HBR is a grating-type device. Grating devices have a long history, which in the context of integrated optics extends back to the late 1960s and 1970s [10]–[15]. Grating-type devices are powerful, but their optimal fabrication requires feature resolution at the level of one to several hundred nanometers combined with spatial coherence (absolute feature placement to substantially better than the in-media wavelength) over the entire structure. In some applications, like the present one, where grating structures of centimeter-scale are desirable, the need to fabricate structures with full spatial coherence has been challenging. In the past, various approaches to grating fabrication have been employed including interferometric optical exposure, e-beam, and frequency-doubling photolithography (not to mention older style mechanical ruling). All of these fabrication approaches have severe limitations. Optical exposure requires spatially coherent optical writing beams having precisely the character needed to write the desired grating. Practically this means that interferometrically written structures have been limited to simple geometries including straight lines and simple curves with regular or no variation between diffractive contours [16]. E-beam fabrication has the required flexibility to write general grating structures but the required coherent field stitching and relatively low writing speed have limited application. E-beam fabrication has been applied to produce small holographic waveguide coupling structures wherein guided modes are coupled to free-space modes and vice versa [17]–[19]. Early application of DUV photolithography via the period-doubling method provided for more complex elliptically shaped focusing gratings, [20], but

the method, being dependent of focal plane image processing, has limited ability to support detailed contour-by-contour variation needed to implement general spectral transfer functions. As mentioned above, elliptic focusing elements provide only rudimentary wavefront transformation capability compared to a general holographic structure and even compared to circular contours which allow flexible imaging between multiple conjugate source and image points.

In the operation of an HBR, optical wavefronts emanate from an effective input port and interact sequentially with the successive HBR diffractive contours. As a wavefront interacts with a particular contour it is reshaped and redirected so as to reach an effective output port. The output wavefronts reaching the output port are the same regardless of which diffractive contour they arise from. Thus each wavefront arriving at the output port via interaction with successive diffractive contours is distinguished by a single quantity, i.e., the effective optical path length from the input port to the diffractive contour and to the output port. Although the diffractive contours and wavefronts are spatially extended, the interaction produces a single effective optical delay. This situation is identical to that found in the case of optical signals interacting with a one-dimensional (1-D) FBG. Thus to tailor the spectral transfer function of the HBR, the methods already developed for FBGs can be immediately applied. It was shown in [1] that the spectral transfer function of the HBR (like the FBG) is related to a Fourier transform of reflectivity versus optical path length in the low reflectivity limit. Advanced spectral design methods applicable for FBGs [21], [22] at high reflectivity can be immediately applied to HBRs. Unlike FBGs (where depth of focus issues limit fabrication flexibility), HBRs can be precisely fabricated with control over the amplitude and phase of individual diffractive contours. When HBRs are fabricated with higher refractive index contrasts and have correspondingly fewer diffractive contours, design algorithms developed for thin-film filters may be utilized in HBR design. The effective gray scale amplitude control method [23] and the control of reflective phase via spatial displacement of contours are fully compatible with simple binary depth photolithographic fabrication.

With precise control over both diffractive amplitude and phase of each of the thousands of diffractive contours involved, one can program the reflection spectrum of the HBR device to have very general properties. In particular, broad and very flat-top reflective bandpass functions difficult to achieve with AWGs can be engineered—without compromising throughput.

### III. DEVICE STRUCTURE AND PERFORMANCE

A two-channel HBR is shown schematically in Fig. 1. In this case, the HBR comprises a 2-D distributed Bragg reflective structure with nanoscale features photolithographically scribed on the upper core-cladding interface of a single-mode planar waveguide.

The present device was fabricated using standard silica-on-silicon deposition, DUV-photolithography, and reactive-ion etching. The core and the cladding thicknesses are 2  $\mu\text{m}$  and 15  $\mu\text{m}$ , respectively. The core-cladding refractive index contrast is  $\sim 0.8\%$  and the depth of the grating elements

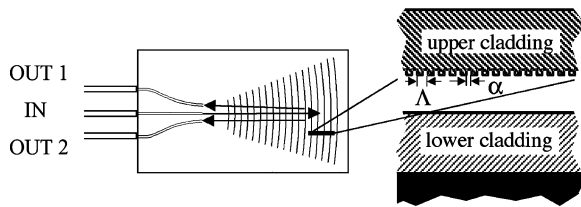


Fig. 1. Left: Schematic top view of HBR. Right: Blow-up cross-sectional schematic of HBR.

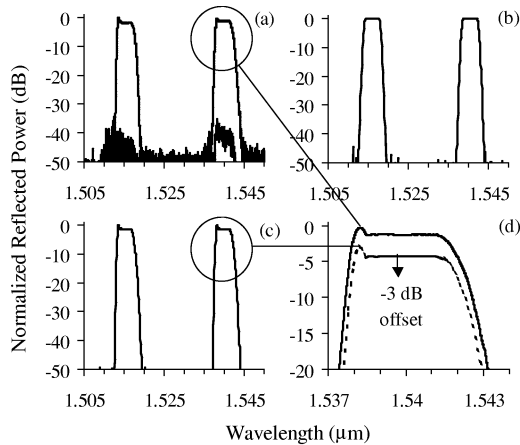


Fig. 2. (a) Measured device throughput versus wavelength. (b) Simulated device throughput versus wavelength with constant  $n_{\text{eff}}$ . (c) Simulated device throughput versus wavelength including variation of  $n_{\text{eff}}$  with amplitude apodization weight. (d) Blow-up comparison of left-most channel in (a) (solid line) and (c) (dashed line); for clarity of comparison, (c) is vertically offset by (-3 dB).

etched into the core is 400 nm. The width of the grating elements ( $\alpha$  in Fig. 1) was roughly 250 nm (50% duty cycle) and the pitch ( $\Lambda$  in Fig. 1) was about 500 nm consistent with first-order Bragg reflection for light in the vicinity of 1.5  $\mu\text{m}$  (vacuum wavelength). Diffractive element contours are nonoptimized circular arcs imaging the common input port onto two distinctive output ports displaced by 60  $\mu\text{m}$  on opposite sides of the input port. Input and output ports comprise channel waveguides that are spaced by 250  $\mu\text{m}$  at the edge of the HBR die. The channel waveguides are adiabatically tapered in width from 12.7  $\mu\text{m}$  at channel-slab waveguide interface to 6  $\mu\text{m}$  at the die edge. For testing, SMF-28 optical fibers were butt-coupled to the channel waveguides at the die edge. The two displaced but partially overlapped HBRs employed in the multiplexer were pie-shaped, about 5 mm in width and 1.1 cm in length, with a lengthwise overlap of  $\sim 0.2$  cm. The individual HBR structures were designed separately and combined on a single reticle.

Fig. 2(a) shows the measured throughput of both channels of the fabricated HBR. The spectrum demonstrates very good channel isolation of  $\sim 40$  dB and steep roll-off. The insertion loss in the center of the passband is found to be 5 dB including a fiber to waveguide coupling loss of about 1 dB. The primary source of loss was low overall reflectivity which can be corrected with simple modification to HBR internal cladding as discussed later.

The HBR employed for each multiplexer channel is chirped to achieve the 4-nm spectral bandpass observed in Fig. 2. To

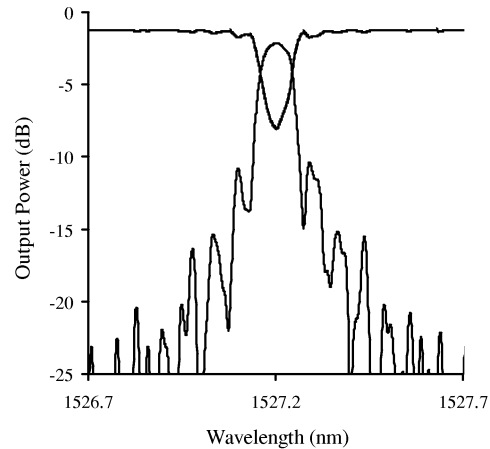


Fig. 3. Measured transmission (top line) and reflection (bottom line) spectrum of a 20-mm-long non-apodized channel waveguide grating. The grating has a reflectivity of 80% and a 3-dB reflection bandwidth of 0.1 nm. This combination of reflectivity and bandwidth requires a coherent grating length of at least 12 mm.

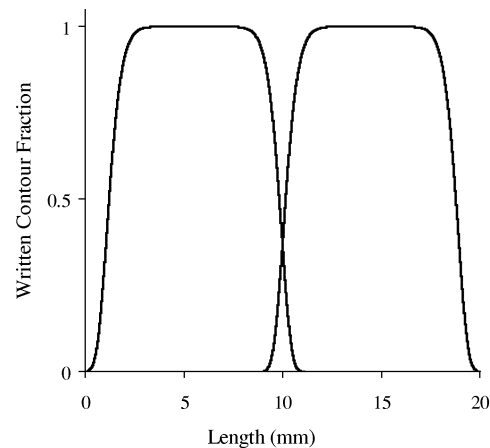


Fig. 4. Amplitude apodization profile for two partially overlain HBRs. Each curve represents a single HBR. HBR structure is summed on the fabrication reticle. No attempt to avoid the occasional intersection of lines from the two HBRs is made although, in refined designs, avoidance of such intersection is desirable.

our knowledge, the present results represent the first implementation of chirp in a focusing 2-D distributed Bragg reflector for passband definition. If the HBRs were not chirped, their 1-cm length would produce an unsaturated 3-dB-linewidth of  $\approx 0.1$  nm. (Tests of an un-chirped grating on the same device (Fig. 3) wafer reveal that the photolithographic methods employed do indeed provide transform-limited spectral response, i.e., have full spatial coherence, for cm-scale devices—an order of magnitude improvement over that demonstrated by previous authors [20].) In addition to the chirp in diffractive element spacing, each HBR was apodized in amplitude and phase to minimize passband ripple. The amplitude apodization was in the form of a super Gaussian ( $\exp(-(x/x_0)^{10})$ ) envelope (Fig. 4). As described elsewhere [23], a novel means of amplitude apodization is introduced by writing each diffractive contour as a series of arcuate segments with the total written fraction of the contour scaled in proportion to the desired reflective amplitude. The achieved passband profile [Fig. 2(a)] closely duplicates the designed passband [Fig. 2(b)] except for a narrow spike on the

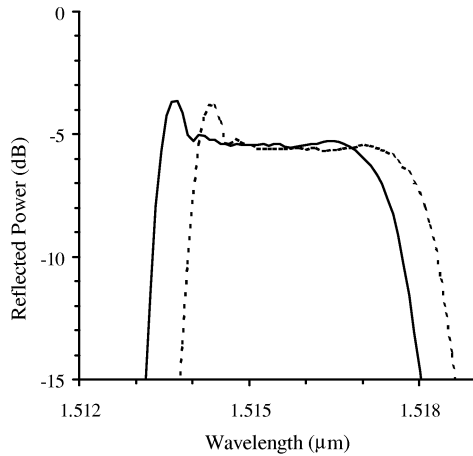


Fig. 5. Measured throughput versus wavelength of fiber-coupled device for two states of polarization: TE (solid line) and TM (dashed line). Extinction ratio between TE and TM polarization was measured to be better than 1:100.

short wavelength side of the passband. We find that the spike results from a coupling of the effective-waveguide refractive index to the amplitude apodization approach employed, i.e., partial scribing of HBR contours. Measurements of separate test structures, confirmed by mode solver simulations, indicated that the effective refractive index of the slab waveguide  $n_{\text{eff}}$  can be approximated in the form

$$n_{\text{eff}} = n_o - 4.5 \times 10^{-4} G(r)$$

where  $G(r)$  is the fraction of each diffractive contour written at each position  $r$  within the device and  $n_o$  is the effective index of the slab waveguide in the absence the HBR contours. Simulations taking this effect into account produced the bandpass profiles of Fig. 2(c), which are in excellent agreement with the measured profile [see detailed comparison of Fig. 2(d)]. Compensating for amplitude-apodization-induced changes in effective waveguide refractive index is easily achieved in HBR design by scaling spatial distances according to the local effective refractive index. Passband profiles are calculated from an explicit spatial model of the HBR structures as they were submitted to the fabrication process. Calculations employed time-consuming but standard Fresnel diffraction methods. These are expected and found to be highly accurate in the weak reflection limit pertaining to the present devices. In accordance with the comments on spectral design made above, the full 2-D Fresnel modeling of spectral transfer functions was found consistent with a simple 1-D model wherein the amplitude and phase of each diffractive contour is parameterized along a single spatial coordinate representing optical path length.

The measurements shown employ polarized input signals. As shown in Fig. 5, polarization-dependent wavelength shifts (PDWL) of  $\sim 0.65$  nm were observed but do not interfere with the wide passbands of interest here or in CWDM generally. Measurements in similar devices having HBRs of differing diffractive orders reveal that PDWL arises from fabrication-related residual stress-induced material birefringence rather than intrinsic HBR function [24]. Small intrinsic PDWL was further confirmed by recently fabricated devices with different layer

architecture and processing procedure demonstrating very small, less than 50 pm, PDWL. The small polarization-dependent change in reflectivity shown in Fig. 5 was found to arise from polarization-dependent coupling between SMF-28 fibers and input channel waveguides, which were rectangular in cross section. It should be noted that the low polarization dependence of the current devices apparently stems from the very low core-cladding refractive index contrast employed (roughly one and a half orders of magnitude less than in [20]).

For applications where multiplexer channels are separated by tens of nanometers and with multi-nanometer passbands (such as CWDM or FTTH), silica-on-silicon HBR devices as described here can be considered essentially polarization and temperature insensitive. Specifically, the design flexibility inherent to the HBR approach allows one to design polarization and temperature insensitive devices by tailoring the multiplexer passband to have small ripple, steep roll-off, and incorporating guardbands to protect against polarization- and temperature-induced wavelength shifts. Assuming that the wavelength shift with temperature,  $\Delta\lambda$ , is caused primarily by the temperature dependence of the refractive index of silica ( $dn/dT = 1.1 \times 10^{-5} \text{ }^\circ\text{C}^{-1}$  [25]), the latter is estimated to be  $\Delta\lambda \sim \pm 0.4$  nm over the operating range of 0 to 70  $^\circ\text{C}$ . Consequently, both temperature- and polarization-dependent shifts represent only a small fraction of a typical CWDM channel bandwidth (13 nm), and hence can be protected against using tractable guardbands.

#### IV. REFLECTIVE STRENGTH AND BANDWIDTH CONSIDERATIONS

HBR devices are reflective in nature. More specifically, they depend on cooperative reflection from distributed arrays of diffractive elements (contours) each of which is by itself a weak scatterer. There are fundamental constraints that connect the total number  $N$  of diffractive elements in an HBR (or alternatively the length  $L$  of the HBR), the diffractive scattering amplitude of each element  $r_a$ , the total spectral bandwidth over which the device is to reflect  $\Delta\nu_{\text{tot}}$ , and the required device insertion loss. Coarse WDM devices (e.g., a 16-channel multiplexer) require high reflectivity over an aggregate bandwidth that may be as large as several hundred nanometers. We wish to estimate the spectral bandwidth (which may or may not be contiguous) over which a first-order HBR of constrained length  $L$  and simple internal geometry can provide high reflectivity. Consider the quarter-wave reflective stack shown in Fig. 6(a) [26]. The stack consists of planar interfaces between materials of refractive indexes  $n_1$  and  $n_2$ . Let  $\Delta n = |n_2 - n_1|$  and  $n = (n_1 + n_2)/2$ . The planar interfaces are spaced by  $\Lambda/2$  and produce strong Bragg backscattering at vacuum wavelength  $\lambda_B = 2n\Lambda$ . The incident wave (assumed incident normal to the interfaces) is attenuated and exhibits a  $1/e$  penetration depth of approximately  $d = n\Lambda/q\Delta n$  [26]. For the quarter-wave stack,  $q = 1$ . The corrugated slab waveguide of Fig. 4(b) exhibits similar behavior except that the factor  $q$ , defined as the ratio of back scattered field amplitudes produced by the corrugation and plane interfaces, is less than one. A regular diffractive structure of length  $d$  has a weak-signal Fourier-transform

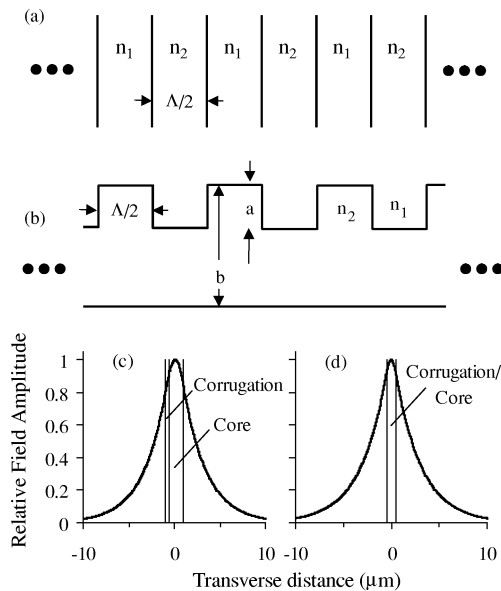


Fig. 6. (a) Quarter-wave stack of planar interfacial reflectors. (b) Corrugated planar waveguide reflector model of HBR. (c) Plot of modal electric field for the corrugated slab waveguide configuration fabricated and tested ( $0.4 \mu\text{m}$  corrugation etched in  $2 \mu\text{m}$  thick waveguide). (d) Plot of the modal electric field for a very broad reflection bandpass slab waveguide structure (see text).

spectral bandpass of approximately  $\Delta\nu_d \approx c/4nd$ , where  $c$  is the vacuum light speed. We use this bandwidth to approximate that of diffractive structures of  $1/e$  field penetration. In the following, we assume that an HBR of length  $L > d$  may be viewed as a number of segments of length  $d$  each of which has bandwidth  $\Delta\nu_d$  and operates at  $1/e$  field transmission. To achieve a broad reflection band, the various HBR segments are chirped or frequency shifted. The construction described is consistent with an overall HBR reflection bandwidth  $\Delta\nu_{\text{tot}}$  given by

$$\Delta\nu_{\text{tot}} = \frac{L}{d} \Delta\nu_d = \frac{cL\Delta n^2 q^2}{4\Lambda^2 n^3}$$

Fig. 6(c) depicts the electric field mode of a corrugated slab waveguide modeled after our fabricated structure. Calculating the field area under the corrugated region and dividing by the total field area, we determine  $q \approx 0.06$ . With  $L = 1 \text{ cm}$ ,  $\Lambda = 0.5 \mu\text{m}$ ,  $n \approx 1.45$ , we get  $\Delta\nu_{\text{tot}} \approx 4 \times 10^{+11} \text{ Hz}$  which corresponds to about a 3-nm reflective bandwidth at the operative wavelength. The present model suggests that the fabricated devices should operate somewhat in the low to moderate reflectivity regime since their bandwidth spanned more than 3 nm—which indeed they were found to do as indicated by their 4 dB reflectivity-limited insertion loss.

We shift our attention to predicting how one might produce an HBR capable of reflecting over several hundred nm as needed for general CWDM mux applications. In Fig. 6(d), we show the modal electric field for a  $1\text{-}\mu\text{m}$ -thick slab waveguide whose corrugations extend entirely through the slab [ $a = b$  in Fig. 6(b)]. The value of  $\Delta n$  has been increased by a factor of three to approximately 0.03. The  $q$  factor is found to be 0.16. With these parameters, we find that  $\Delta\nu_{\text{tot}} \approx 3 \times 10^{+13} \text{ Hz}$ , which corresponds to about a 210-nm reflective bandwidth at

the operative wavelength—broad enough to support sixteen 13-nm-wide CWDM channels. It should be noted the etch aspect-ratio needed to produce the described broadband HBR device has been demonstrated as part of the LightSmyth development program. Note further that a wide range of HBR internal designs are possible providing even broader reflection bands and fully consistent with low loss at the fiber to die interface. It appears entirely possible to integrate much of the current functionality attributed to discrete thin-film filters into the fully integrated environment.

## V. SUMMARY

Harnessing the ever more-widely available DUV photolithographic fabrication capabilities developed for the electronics industry, and planar device fabrication processes refined largely in the context of AWGs, we have demonstrated a powerful integrated approach to some filtering/multiplexing applications now handled exclusively or nearly so by discrete TFFs. We have further presented a simple model suggesting that very broadband and widely configurable filters will be possible. We note that in CWDM applications, silica-on-silicon planar waveguide HBR devices will not require temperature control. Also polarization-dependent passband shifts produced by residual material birefringence are not a serious design issue. The HBR integrated photonic device approach promises, through ultimate stamping/embossing-based fabrication, to support a uniquely low cost approach to producing filtering devices for coarse WDM, access WDM, and even datacom.

## REFERENCES

- [1] T. W. Mossberg, "Planar holographic optical processing devices," *Opt. Lett.*, vol. 26, no. 7, pp. 414–416, Apr. 2001.
- [2] —, "Lithographic holography in planar waveguides," *SPIE Holography Newsl.*, vol. 12, no. 2, p. 1, 8, Nov. 2001.
- [3] T. Erdogan, "Fiber grating spectra," *J. Lightwave Technol.*, vol. 15, pp. 1277–1294, Aug. 1997.
- [4] C. R. Giles, "Lightwave application of fiber Bragg gratings," *J. Lightwave Technol.*, vol. 15, pp. 1391–1404, Aug. 1997.
- [5] V. Mizrahi, T. Erdogan, D. J. DiGiovanni, P. J. Lemaire, W. M. MacDonald, S. G. Kosinski, S. Cabot, and J. E. Sipe, "Four channel fiber grating demultiplexer," *Electron. Lett.*, vol. 30, no. 10, pp. 780–781, May 1994.
- [6] M. K. Smith and C. van Dam, "PHASAR-based WDM-devices: Principles, design, and applications," *IEEE J. Select. Topics Quantum Electron.*, vol. 2, pp. 236–250, June 1996.
- [7] Y. Inoue *et al.*, "Low-crosstalk 4-channel coarse WDM filter using silica-based planar lightwave circuit," *Opt. Fiber Commun. Conf. 2002*, pp. 75–76, Mar. 17–22, 2002.
- [8] H. Sasaki and Y. Okabe, "CWDM multi/demultiplexer consisting of stacked dielectric interference filters and off-axis diffractive lenses," *IEEE Photon. Technol. Lett.*, vol. 15, pp. 551–553, Apr. 2003.
- [9] Y. Hibino, "Recent advances in high-density and large-scale AWG multi/demultiplexers with higher index-contrast silica-based PLCs," *IEEE J. Select. Topics Quantum Electron.*, vol. 8, pp. 1090–1101, Nov. 2002.
- [10] P. K. Tien, "Light waves in thin films and integrated optics," *Appl. Opt.*, vol. 10, p. 2395, 1971.
- [11] A. Yariv, "Coupled-mode theory for guided-wave optics," *IEEE J. Quantum Electron.*, vol. QE-9, p. 919, 1973.
- [12] K. Ogawa, W. S. C. Chang, B. L. Sopori, and F. J. Rosenbaum, "A theoretical analysis of etched grating couplers for integrated optics," *IEEE J. Quantum Electron.*, vol. QE-9, p. 29, 1973.
- [13] C. C. Ghizoni, B. Chen, and C. L. Tang, "Theory and experiments on grating couplers for thin-film waveguides," *IEEE J. Quantum Electron.*, vol. QE-12, p. 69, 1976.

- [14] W. Rigrod and D. Marcuse, "Radiation loss coefficients of asymmetric dielectric waveguides with shallow sinusoidal corrugations," *IEEE J. Quantum Electron.*, vol. QE-12, p. 673, 1976.
- [15] A. Yariv and M. Nakamura, "Periodic structures for integrated optics," *IEEE J. Quantum Electron.*, vol. QE-13, p. 233, 1977.
- [16] P. K. Tien, "Method of forming novel and curved-line gratings and their use as reflectors and resonators in integrated optics," *Opt. Lett.*, vol. 1, p. 64, 1977.
- [17] M. Li, M. Hagberg, J. Bengtsson, N. Eriksson, and A. Larsson, "Optical waveguide fan-out elements using dislocated gratings for both out-coupling and phase shifting," *IEEE Photon. Technol. Lett.*, vol. 8, pp. 1199–1201, Sept. 1996.
- [18] M. Li, J. Bengtsson, M. Hagberg, A. Larson, and T. Suhara, "Off-plane computer generated waveguide hologram," *IEEE J. Select. Topics Quantum Electron.*, vol. 2, pp. 226–235, June 1996.
- [19] J. Backlund, J. Bengtsson, C. Carlstrom, and A. Larsson, "Input waveguide grating couplers designed for a desired wavelength and polarization response," *Appl. Opt.*, vol. 41, pp. 2818–2825, May 2002.
- [20] C. H. Henry, R. F. Kazarinov, Y. Shani, R. C. Kistler, V. Pol, and K. J. Orlovsky, "Four-channel wavelength division multiplexers and bandpass filters based on elliptical Bragg reflectors," *J. Lightwave Technol.*, vol. 8, no. 5, pp. 748–755, May 1990.
- [21] R. Feced, M. N. Zervas, and M. A. Muriel, "An efficient inverse scattering algorithm for the design of nonuniform fiber Bragg gratings," *IEEE J. Quantum Electron.*, vol. 35, pp. 1105–1115, Aug. 1999.
- [22] J. Skaar, L. Wang, and T. Erdogan, "On the synthesis of fiber Bragg gratings by layer peeling," *IEEE J. Quantum Electron.*, vol. 37, pp. 165–173, Feb. 2001.
- [23] D. Iazikov, C. Greiner, and T. W. Mossberg, "Effective gray-scale in lithographically-scribed planar holographic Bragg reflectors," *Appl. Opt.*, vol. 43, pp. 1149–1155, Feb. 2004.
- [24] C. Greiner, D. Iazikov, and T. W. Mossberg, "Lithographically-fabricated planar holographic Bragg reflectors," *J. Lightwave Technol.*, vol. 22, pp. 136–145, Jan. 2004.
- [25] K. Okamoto, *Fundamentals of Optical Waveguides*. San Diego, CA: Academic, 2000.
- [26] A. Yariv and P. Yen, *Optical Waves in Crystals*. New York: Wiley, 1983.



**D. Iazikov** (M'03) was born in St. Petersburg, Russia, in 1971. He received the B.S. and M.S. degrees in applied optics from the Moscow University of Physics and Technology, Moscow, Russia, in 1990 and 1993, respectively.

He has been involved in the development of optical components and systems since 1990 and has recently held positions as Design Authority at JDS Uniphase's thin-film-filter-based wide-band WDM group and as Technical Lead for AWG and OADM development at Zenastra Photonics. Since joining LightSmyth Technologies as a Senior Scientist in 2002, he has been engaged in the design and characterization of holographic Bragg reflector-enabled planar lightwave circuits.

Dr. Iazikov is a Member of the the International Society for Optical Engineers (SPIE).



**C. Greiner** received the M.A. and Ph.D. degrees in optical physics from the University of Oregon, Eugene, in 1995 and 2002, respectively.

He has been a Senior Scientist with LightSmyth Technologies, Eugene, OR, since 2002. Presently, his main research interests concern the development of integrated photonic components based on planar holographic Bragg reflectors.

Dr. Greiner is a Member of the American Physical Society, the German Physical Society, the Optical Society of America (OSA), and the International Society for Optical Engineers (SPIE).



**T. W. Mossberg** (M'96) received the B.A. degree from the University of Chicago, Chicago, IL, in 1973 and the M.A. and Ph.D. degrees from Columbia University, New York, in 1975 and 1978, respectively.

He has served on the faculties of Columbia University, Harvard University, and the University of Oregon. He has published approximately 140 refereed technical articles treating optics and physics. During the mid-1990s, he co-founded Templex Technologies and is currently CTO of LightSmyth Technologies, Eugene, OR, specializing in the design and fabrication of planar holographic optical devices and distributed photonic circuits.

Dr. Mossberg is a Fellow of the American Physical Society and the Optical Society of America (OSA) and a Member of the International Society for Optical Engineers (SPIE).